



# The influence of burial heating on the (U–Th)/He system in apatite: Grand Canyon case study



Matthew Fox<sup>a,b,\*</sup>, David L. Shuster<sup>a,b</sup>

<sup>a</sup> Department of Earth and Planetary Science, University of California, Berkeley, CA 94720, USA

<sup>b</sup> Berkeley Geochronology Center, 2455 Ridge Road, Berkeley, CA 94709, USA

## ARTICLE INFO

### Article history:

Received 1 March 2014

Received in revised form 22 April 2014

Accepted 23 April 2014

Available online xxxx

Editor: T.M. Harrison

### Keywords:

apatite (U–Th)/He thermochronology

radiation damage

Grand Canyon incision

## ABSTRACT

Thermochronological data can constrain the cooling paths of rocks exhumed through the uppermost 1–2 km of earth's crust, and have thus been pivotal in illuminating topographic development over timescales  $>0.1$  Ma. However, in some cases, different methods have led to conflicting conclusions about timing of valley-scale exhumation. Here, we investigate the case of Western Grand Canyon, USA, where different thermochronological datasets have been interpreted to record very different timings of canyon incision ( $\sim 70$  Ma versus  $\sim 5$  Ma). We present a method to assess key assumptions in these constraints and demonstrate that burial heating conditions of basement rocks in the Mesozoic can result in incomplete annealing of radiation damage in apatite. In turn, this has a dramatic effect on the temperature sensitivity of the apatite (U–Th)/He system and its ability to record post-burial exhumation. The possibility of incomplete annealing resolves the apparent conflict in time-temperature paths inferred over the last 70 Ma, although it requires temperatures during burial that are lower than predicted by apatite fission track data. A refinement of parameters that prescribe the kinetics of damage annealing and related control on  $^4\text{He}$  diffusivity in apatite would account for this discrepancy, specifically if alpha recoil damage anneals at a lower rate than fission tracks at a given temperature. These effects will be important for any application of the apatite (U–Th)/He system in geologic settings that experienced prolonged residence ( $>10$  Ma) between 50–150 °C; the approaches developed here provide means to assess these effects.

© 2014 Elsevier B.V. All rights reserved.

## 1. Introduction

Helium-based thermochronometry in apatite has sensitivity to temperatures  $\sim 90$ – $30$  °C (Zeitler et al., 1987; Farley, 2000; Shuster et al., 2006; Flowers et al., 2009), corresponding to crustal depths equivalent to the height of mountainous topography (House et al., 1998; Ehlers and Farley, 2003). This sensitivity to relatively low temperatures has enabled geomorphic applications that have quantified rates and patterns of erosion associated with both glacial processes (e.g., Spotila et al., 2004; Ehlers et al., 2006; Shuster et al., 2011; Valla et al., 2011; Glotzbach et al., 2011) and fluvial canyon incision (e.g., Schildgen et al., 2010; Flowers and Farley, 2012). These processes, however, may represent only the most recent phase of local bedrock exhumation, whereas the ultimate temperature sensitivity of the apatite (U–Th)/He system may be influenced by geologic processes operating over a much longer time interval, including sedimentary burial and associated

increases in temperature. Details of the entire thermal history may significantly influence the kinetics of  $^4\text{He}$  diffusion through time, especially for samples that experienced anything other than solely decreasing temperatures (Shuster et al., 2006; Flowers et al., 2009; Gautheron et al., 2009), hence leading to additional uncertainty in the final episodes of cooling that are constrainable by (U–Th)/He data. Further, burial to depths of order 1–3 km in sedimentary basins is often associated with temperatures that may only partially reset both previously accumulated radiogenic  $^4\text{He}$  and the temperature sensitivity of the apatite (U–Th)/He system. This poses a challenge to the use of low-temperature thermochronometry to quantify recent km-scale exhumation of sedimentary deposits.

Open system behavior in the (U–Th)/He system occurs in the range  $\sim 90$ – $30$  °C in apatite due to a competition between production and thermally activated diffusive loss of radiogenic  $^4\text{He}$  (Farley, 2000; Shuster et al., 2006). The apatite (U–Th)/He age therefore provides a non-unique constraint on the time transpired since a sample cooled below these temperatures; a large range of time-temperature paths will be consistent with a given apatite (U–Th)/He age. Through stepwise degassing analysis of samples containing a spatially uniform distribution of proton-induced  $^3\text{He}$ ,

\* Corresponding author. Tel.: +510 644 0225.

E-mail address: matthew.fox@berkeley.edu (M. Fox).

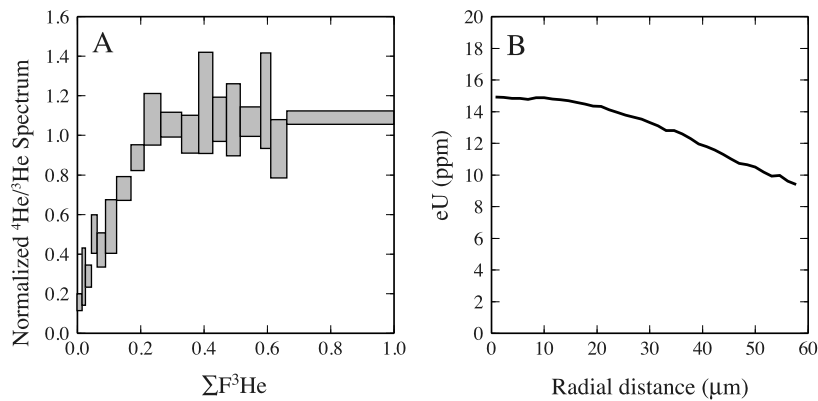


**Fig. 1.** Stepwise  $^4\text{He}/^3\text{He}$  release spectrum and eU zonation representation for sample CP06-69D from the Grand Canyon (Flowers and Farley, 2012). (A) Normalized  $^4\text{He}/^3\text{He}$  spectrum diagram. The x-axis is cumulative release fraction of proton-induced  $^3\text{He}$ ; y-axis is the  $R_{\text{step}}/R_{\text{bulk}}$  value (where  $R$  is the ratio of  $^4\text{He}/^3\text{He}$ ) normalized by a synthetic equivalent ratio calculated for the non-diffusive  $^4\text{He}$  production function. (B) Concentration of [eU] as a function of radial distance from the center of the grain. The conversion of 2D spatial eU concentration maps to 1D radial symmetric concentrations is following Farley et al. (2011). The solid line shows the weighted average.

$^4\text{He}/^3\text{He}$  thermochronometry provides observations that reflect the spatial distribution of  $^4\text{He}$  within an apatite crystal (Shuster and Farley, 2004). These data restrict the number of time-temperature paths a sample could have experienced. However, in addition to time and temperature, the spatial distribution of  $^4\text{He}$  depends also on probabilistic emission of alpha particles from a crystal's exterior (Farley et al., 1996) and the spatial distribution of U and Th within the crystal (Farley et al., 2010). Therefore, methods have been developed to measure the spatial distribution of U and Th within apatite using laser ablation inductively coupled plasma mass spectrometry (LA-ICPMS; Farley et al., 2011). The combination of  $^4\text{He}/^3\text{He}$  analysis with a measure of the spatial variations in  $^4\text{He}$  increases accuracy of inferred time-temperature paths.

The diffusivity of  $^4\text{He}$  in apatite is a function of temperature, time and the concentration of effective U, [eU], in the crystal ( $[\text{eU}] = [\text{U}] + 0.24[\text{Th}]$ ), which weights the U and Th concentrations according to their relative alpha particle productivity; Flowers et al., 2009). In particular, the radioactive decays along U- and Th-decay chains produce alpha-recoil “radiation damage” within the apatite crystal lattice. At sufficiently low temperatures, the accumulation of such damage has been observed to cause the effective He diffusivity in apatite to decrease over time at a given temperature (Shuster et al., 2006). At sufficiently high temperatures, any accumulated damage sites will “anneal”, returning back to a crystalline state and returning He diffusivity to higher values at a specific temperature (Shuster and Farley, 2009). By analyzing different apatite crystals spanning a range of U and Th concentrations and a range of thermal histories, models have been developed that account for variations in  $^4\text{He}$  retentivity as a function of accumulation and annealing of radiation damage (Shuster et al., 2006; Flowers et al., 2009; Gautheron et al., 2009). For example, the radiation damage accumulation and annealing model (RDAAM) is an empirically calibrated model that assumes the kinetics of damage annealing (i.e., that influences He diffusivity) can be quantified by the same calibrated kinetic functions that describe fission track annealing in apatite (Flowers et al., 2009). The model contains two interconnected functions: one that quantifies the temperature dependence of damage annealing, and one the temperature dependence of  $^4\text{He}$  diffusion.

These effects involving radiation damage accumulation and annealing mean that details of a sample's prior thermal state will control  $^4\text{He}$  diffusivity at any given point in time. An important implication is that any uncertainty in prior thermal conditions will therefore produce additional uncertainty in the most recent phase of exhumation that can be constrained by the (U–Th)/He system. If a rock can be assumed to have only experienced cooling to the surface (as is often the case in deeply eroded plutonic terranes;

e.g., Shuster et al., 2005), these complicating effects are minimized and the system has highest resolving power at low temperatures ( $<80^\circ\text{C}$ ). The RDAAM's sensitivity to reheating has been previously shown to produce diagnostic “age-[eU] correlations” that have been observed in several cases (e.g., Flowers et al., 2009; Flowers, 2009; Fillon et al., 2013; Ault et al., 2009; Gautheron et al., 2013). However, numerical methods quantifying the effects of burial temperature and duration uncertainties upon the most recent valley-scale exhumation have not been fully established.

A notable example of conflicting time-temperature paths inferred from (U–Th)/He and apatite fission track (AFT) datasets are those for samples from the base of Western Grand Canyon (Flowers et al., 2008; Flowers and Farley, 2012; Lee et al., 2013). The conflicting interpretations indicate there may be additional aspects of  $^4\text{He}$  diffusivity and/or fission track annealing in apatite that are not sufficiently understood. Incision of Grand Canyon is postulated to have caused a cooling signature that is resolvable with apatite (U–Th)/He and AFT data (Flowers et al., 2008; Flowers and Farley, 2012; Lee et al., 2013). Fission track data require that portions of the canyon formed at different times (Lee et al., 2013; Karlstrom et al., 2014), yet supports the hypothesis that Western Grand Canyon formed within the last 5–6 Ma (Karlstrom et al., 2013). However,  $^4\text{He}/^3\text{He}$  thermochronometric data, combined with LA-ICPMS data (Fig. 1) suggest that Western Grand Canyon was incised to its current canyon relief and at the current stratigraphic level at  $\sim 70$  Ma (Flowers and Farley, 2012). Since this lack of internal consistency highlights a limitation and challenge for these methods of thermochronometry, we use this geologic setting and data to explore the effects of heating during burial on the (U–Th)/He system. In particular, we focus on the potential of  $^4\text{He}/^3\text{He}$  release spectra to constrain Grand Canyon incision, given the uncertainty in heating conditions during burial. To this end, we develop a method that explores the relationship between burial uncertainty and subsequent valley exhumation uncertainty using recently published data from the Grand Canyon as an example. In addition, we explore sensitivity of RDAAM to changes in the parameters controlling the annealing of radiation damage.

## 2. Method: numerical model

In order to explore the effects of long-term reheating on the (U–Th)/He system in apatite, we simulate the evolution of (U–Th)/He age and the closure temperature ( $T_c$ ; Dodson, 1973). For these calculations we use a numerical model to solve the  $^4\text{He}$  production diffusion-equation using a spherical approximation (Fechtig and Kalbitzer, 1966). Our model accounts for spatially symmetric U and Th zonation within apatite on the production

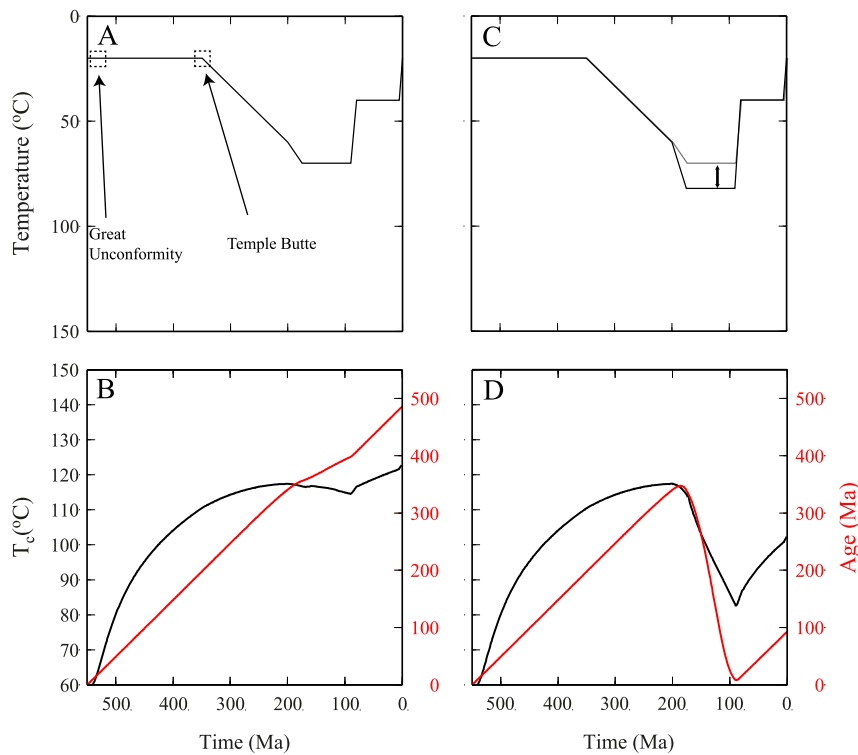


**Fig. 2.** The evolution of apparent (U–Th)/He age and of closure temperature,  $T_c$ . (A) Illustrative time–temperature path simulating near surface temperatures as indicated by the Great Unconformity and the Temple Butte constraint, a burial event to intermediate temperatures, followed by a characteristic young canyon model. (B) Evolution of age and closure temperature through time. The value of  $T_c$  is calculated from the evolving  ${}^4\text{He}$  diffusion kinetics predicted by RDAAM (Flowers et al., 2009) assuming a uniform [eU] value of 40 ppm and referenced to  $dT/dt = 10^\circ\text{C}/\text{Ma}$ . (C) The same time–temperature path as in (A) except the peak temperature during burial has been increased to  $85^\circ\text{C}$ . (D) The evolution of apparent (U–Th)/He age and of closure temperature referenced to a cooling rate of  $10^\circ\text{C}/\text{Ma}$  for the time–temperature path shown in (C).

rate of  ${}^4\text{He}$ , alpha ejection and also diffusivity, as outlined in Ketcham (2005). We assume the concentration of  ${}^4\text{He}$  at the grain boundary is equal to 0 and that there is no  ${}^4\text{He}$  flux across the center of the grain. We discretize grain radius into units of constant length (typically  $0.5\ \mu\text{m}$ ) and solve the  ${}^4\text{He}$  production diffusion equation using the Crank–Nicolson finite-difference scheme (Ketcham, 2005). The evolution of diffusivity as a function of space within the crystal and time is calculated according to observed [eU] zonation data and the RDAAM of Flowers et al. (2009). For all simulations we use parameter set 2 in RDAAM (Flowers et al., 2009).

To calculate  $T_c$ , we require knowledge of the activation energy ( $E_a$ ) and frequency factor ( $D_0/a^2$ ). However, due to the accumulation and annealing of radiation damage, these quantities vary through time (Shuster et al., 2006; Flowers et al., 2009). Therefore, to calculate the evolution in  $T_c$ , we model a synthetic degassing experiments at 1 Ma intervals for the specified thermal history. A linear regression through the synthetic Arrhenius plot quantifies the effective  $E_a$  and  $D_0/a^2$ , which are then used to calculate  $T_c$  from Dodson’s equation using a reference cooling rate of  $10^\circ\text{C}/\text{Ma}$  and radius of  $60\ \mu\text{m}$  (Dodson, 1973; Reiners and Brandon, 2006). Importantly, since the thermal path does not involve a constant cooling rate, this is not representative of the actual closure temperature, but used as an intuitive parameter that represents changes in diffusion kinetics through time.

### 3. Results and discussion: general system behavior

#### 3.1. Evolution of retentivity and apparent age

To quantify the effects of burial heating on the apatite (U–Th)/He system, we use the time–temperature path in Fig. 2B to predict evolution of the (U–Th)/He age and  $T_c$ . This time–temperature

path is chosen to highlight the effects of radiation damage accumulation and annealing. In the simulated time–temperature path, rocks resided at near surface temperatures between 550 and 350 Ma to model an accumulation of radiation damage effects over a long geologic time interval prior to subsequent burial heating. We then initially set the peak temperature during burial to  $70^\circ\text{C}$  between 190 and 90 Ma. We then initially set the peak temperature during burial to  $70^\circ\text{C}$  between 190 and 90 Ma, Fig. 2A. A uniform [eU] value of 40 ppm is used for this calculation. Fig. 2B shows that  $T_c$  increases over the first 250 Ma of this simulated path at low temperature (from 550 to 350 Ma), before reaching values  $>110^\circ\text{C}$  [for reference, the canonical  $T_c$  of Durango apatite is  $68^\circ\text{C}$  (Farley, 2000)]. Since diffusive loss of  ${}^4\text{He}$  is negligible along much of the path, age increases nearly linearly throughout the simulation. The peak burial temperature of  $70^\circ\text{C}$  has a negligible effect on  $T_c$ , and the rate of increase in apparent age decreases slightly due to  ${}^4\text{He}$  loss. The resistance to diffusive  ${}^4\text{He}$  loss results from increased  ${}^4\text{He}$  retentivity due to radiation damage accumulation. As the temperature between open and closed system behavior increases due to increased radiation damage, the sensitivity of the data to km-scale exhumation is reduced as shown by the evolution of closure temperature.

However, if the peak temperature is slightly increased from 70 to  $85^\circ\text{C}$  between 190 and 90 Ma (Fig. 2C), the evolution of age and  $T_c$  is very different (Fig. 2D); the (U–Th)/He age would decrease sharply due to an elevated  ${}^4\text{He}$  diffusivity. However, while this burial condition predicts complete resetting of the (U–Th)/He age to 0 Ma, the diffusion kinetics (and  $T_c$ ) are not completely reset to pre-radiation values. Even at  $85^\circ\text{C}$  for 100 Ma, the rate of radiation damage annealing predicted by RDAAM is relatively low. This is important, since this scenario predicts complete resetting of the (U–Th)/He age while maintaining a relatively high  $T_c$ , or low sensitivity to recording subsequent km-scale exhumation.

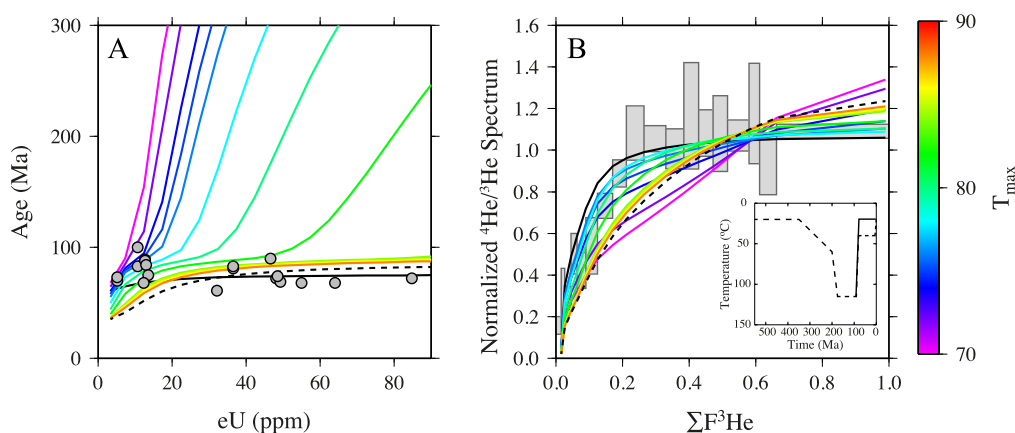


**Fig. 3.** Sensitivity of (U–Th)/He and  $^4\text{He}/^3\text{He}$  thermochronometers to reheating during burial. The form of the time–temperature paths used for these calculations is the same as in Fig. 2. However, the maximum temperatures ( $T_{max}$ ) during burial are adjusted by modifying the portion of the time–temperature path as shown in Fig. 2C. (A) variations in the age–[eU] relationship due to systematically varying  $T_{max}$  during reheating. (B) effects of the normalized  $^4\text{He}/^3\text{He}$  spectrum due to varying  $T_{max}$ . The black dashed and solid curves correspond to the reference time–temperature paths shown in the inset. For reference, the parameter controlling annealing of radiation damage ( $r_{m0}$ ) is set to the canonical value of 0.83 (Ketcham et al., 2007). (For interpretation of the references to color in this figure, the reader is referred to the web version of this article.)

### 3.1.1. Effects of reheating on apatite (U–Th)/He age and [eU] correlation

The influence of radiation damage accumulation on the (U–Th)/He system’s sensitivity to geologic reheating has previously been investigated (Shuster et al., 2006; Flowers et al., 2009; Gautheron et al., 2009). Here, we more broadly explore the relationships between uncertainty in temperatures of burial reheating and the resulting uncertainty in subsequent exhumation constraints. To illustrate such relationships, we use the (U–Th)/He thermochronometric dataset from the Western Grand Canyon [samples CP06-65, CP06-69 and CP0671A (Flowers et al., 2008) and GC863 (Flowers and Farley, 2012)] and the representative time–temperature path from Fig. 2 as a basis for our analysis, but systematically vary the peak temperature to model different depths of maximum burial between 190 and 90 Ma ago. Predictions for two additional time–temperature paths are shown for reference. The first reference time–temperature path reaches 115°C during reheating and the cooling history over the last 90 Ma is identical to the path shown in Fig. 2. The age–[eU] relationship predicted for this path is shown as a dashed line in Fig. 3. The second reference path also reaches 115°C during reheating, but then cools to 20°C at 80 Ma; this path is represented by a solid black line in Fig. 3. Both reference paths lead to complete annealing of radiation damage and diffusive loss of  $^4\text{He}$  during reheating. For this calculation, we use a spherical crystal approximation with a radius of 70  $\mu\text{m}$  and a spatially uniform distribution of [eU].

The effects of peak temperature on the predicted (U–Th)/He ages as a function of [eU] is shown in Fig. 3A. Due to variations in radiation damage accumulation, apatite crystals with different [eU] have developed different sensitivity to diffusive  $^4\text{He}$  loss at elevated burial temperatures. Therefore, grains with high [eU] have higher retentivity and thus retain previously-accumulated  $^4\text{He}$  at the same temperatures sufficient to completely degas apatites with low [eU]. At higher temperatures, pre-burial  $^4\text{He}$  is progressively lost from apatites with higher [eU], while increased annealing of radiation damage resets all apatites to lower  $T_c$  leaving crystals with low [eU] very sensitive to subsequent thermal conditions.

The temperature sensitivity of the age–[eU] curves of Fig. 3A depends on the fundamental assumption of the RDAAM that annealing of alpha-recoil damage (i.e., the primary control on time-dependent  $^4\text{He}$  diffusivity; Shuster et al., 2006; Shuster and Farley, 2009) is analogous to the annealing of fission tracks (Flowers et al., 2009). The difference between the temperature dependence of damage annealing and  $^4\text{He}$  diffusivity predicts that annealing of radiation damage will occur in crystals with low [eU] prior to diffusive loss of  $^4\text{He}$  for crystals with high [eU]. Furthermore, an-

nealing of radiation damage occurs prior to diffusive loss of  $^4\text{He}$  for crystals with significant amounts of radiation damage. Therefore,  $^4\text{He}$  is lost for crystals with high [eU] due to the annealing of radiation damage and the resulting change in temperature sensitivity. If at a given temperature the annealing of alpha-recoil damage occurs at a lower rate than fission track damage annealing, the age–[eU] relationship for a specific time–temperature path would not be as sensitive to the narrow temperature range in  $T_{max}$  and the predicted curves would be very different, as discussed below. Therefore, any uncertainties in RDAAM propagate directly into uncertainty in the temperature sensitivity, and small changes in peak temperature during reheating will lead to large differences in age–[eU] curves.

### 3.1.2. Effects of reheating on apatite $^4\text{He}/^3\text{He}$ thermochronometry in general

Next, we illustrate the effects of reheating on apatite  $^4\text{He}/^3\text{He}$  He release spectra for the illustrative time–temperature paths in Fig. 2A, and use the same range of peak temperatures used to calculate Fig. 3A. For these calculations, and for comparison with published data, we use the zonation data for crystal CP06-69D (Flowers and Farley, 2012), shown in Fig. 1B. The predicted (U–Th)/He age for the simulated history is equal to the predicted age for a crystal with a bulk [eU] of approximately 15 ppm.

At relatively low maximum burial temperatures (<75°C), a portion of the previously accumulated  $^4\text{He}$  is retained and the final  $^4\text{He}/^3\text{He}$  spectrum largely reflects diffusive loss during burial (Fig. 3B). At slightly higher burial temperatures (~75–85°C), nearly all of the previously accumulated  $^4\text{He}$  is lost during burial, but the radiation damage effect on diffusivity is not completely reset. This means that after these burial conditions, the transition between the open to closed behavior of the (U–Th)/He system occurs at elevated temperatures. This results in a normalized  $^4\text{He}/^3\text{He}$  spectrum that is characteristic of a crystal that has resided for a long duration at temperatures at which  $^4\text{He}$  is completely retained and the system is closed, i.e., a steep profile during the initial heating steps that flattens out after approximately 25% of the reference  $^3\text{He}$  has been released. At burial temperatures >85°C, an increasing proportion of radiation damage is annealed, such that the sample as a whole – and especially the outermost low [eU] region of CP06-69D – is increasingly sensitive to diffusive loss of  $^4\text{He}$  at very low temperatures after 90 Ma. For example, following burial temperatures >85°C, an assumed temperature of 40°C between 90 and 6 Ma results in a strongly diffusive  $^4\text{He}$  distribution (Fig. 3B). It is important to note that these conditions also predict a young

(U–Th)/He age for the crystal and that this influence on the (U–Th)/He age is the first order effect.

The predicted normalized  $^4\text{He}/^3\text{He}$  spectra for the two reference time-temperature paths are also shown in Fig. 3B. The first reference path predicts a diffusive  $^4\text{He}$  profile due to the long duration spent at 40 °C during the last 80 Ma. Conversely, the second reference path predicts a less-diffusive  $^4\text{He}$  profile due to the very low temperatures over the last 80 Ma. This latter profile is similar to that predicted for a time-temperature path in which radiation damage is not completely annealed.

Finally diffusive loss of  $^4\text{He}$  and radiation damage annealing also depend on the heating duration. In the subsequent section we extend the analysis to incorporate the effects of variable durations of burial heating.

#### 4. Results and discussion: potential of $^4\text{He}/^3\text{He}$ data to resolve Grand Canyon incision

##### 4.1. Grand Canyon background

Determining the timing and rate of Grand Canyon incision has been a long-standing challenge of the last 150 years (e.g. Powell, 1875). Attempts to quantify the timing of incision have involved dating the arrival of Grand Canyon derived detritus (Faulds et al., 2001; Lucchitta, 2013; Dorsey et al., 2007; Ingersoll et al., 2013), geochronology of basalt flows that drape topography or are found on opposite sides of canyons (Lucchitta and Jeanne, 2001) and dating sediments that were transported across the canyon prior to incision (Young, 1989). These studies generally support a “young” canyon model in which much of Western Grand Canyon became integrated and incised to its current depth ~5–6 Ma ago. However, several of the key geological constraints have been questioned based on additional complexities and alternative datasets (Polyak et al., 2008; Hill and Ranney, 2008; Spencer and Pearthree, 2001).

A competing “old” Grand Canyon model has also been proposed in which Grand Canyon was formed as part of an earlier drainage system that flowed toward the northeast (e.g. Potochnik, 2001; Young, 2001, 2008). In this model Grand Canyon persisted in its present location, and depth since ~70 Ma ago. Studies supporting the old canyon model suggest that an east-flowing river at ~70–80 Ma was followed by a west-flowing river ~30–55 Ma ago that incised a canyon in the same location and of nearly the same depth as modern Grand Canyon. Then much later, this abandoned paleocanyon was re-used opportunistically by the west-flowing Colorado River *en route* to the Gulf of California (Wernicke, 2011; Flowers et al., 2009; Flowers and Farley, 2012). In this model, the Colorado River did not play a significant role in excavating Grand Canyon, and surface uplift of the Colorado Plateau took place in the Laramide (Flowers et al., 2008; Wernicke, 2011).

Reconciling these conflicting conclusions is important, as the incision of Grand Canyon has been used to constrain mantle dynamics and uplift of the Colorado Plateau (Moucha et al., 2008; Karlstrom et al., 2012; Roberts et al., 2012) and landscape evolution models (Howard et al., 1994). These contrasting interpretations of data also enable us to test our quantitative understanding of the kinetics of both the (U–Th)/He and fission track systems in apatite.

##### 4.2. Independent time-temperature constraints

The basement rocks of Grand Canyon are some of the oldest on Earth and, as noted by Powell (1875), the sedimentary sequence above the basement is cut by several unconformities that indicate a complex thermal history. The unconformity representing the longest gap in the stratigraphic record is the

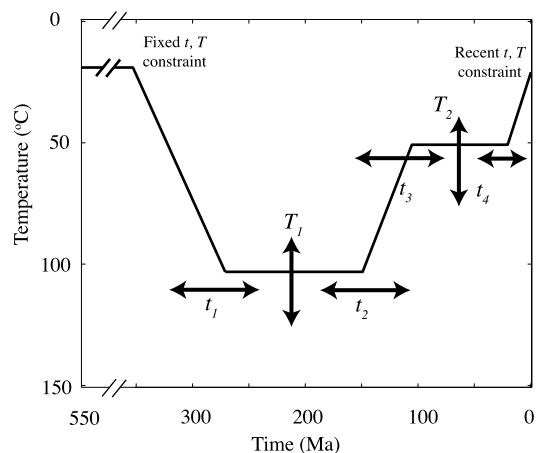


Fig. 4. Parameterization of explored time-temperature space showing the free model parameters.  $T_1$  is the temperature between  $t_1$  and  $t_2$  and  $T_2$  is the temperature between  $t_3$  and  $t_4$ . Both an old and young canyon model are permitted by the range of prior values on these parameters. Variations in  $T_1$  simulate heating to different temperatures during burial and the duration of heating is controlled by  $t_1$  and  $t_2$ . The ranges of permitted values for the temperature parameters,  $T_1$  and  $T_2$ , are from 20 to 150 °C. The ranges for  $t_1$ – $t_4$  are defined as follows:  $t_1 = 150$ –300 Ma;  $t_2 = 86$ –145 Ma;  $t_3 = 30$ –85 Ma; and,  $t_4 = 3$ –25 Ma.

Great Unconformity. The Great Unconformity separates the basement from the overlying sedimentary rocks, providing evidence that the basement rocks were exposed to erosion, and thus at surface temperatures, ~540 Ma ago (Karlstrom and Timmons, 2012). The basement rocks were also close to Earth’s surface (<0.5 km) ~359 Ma ago, identified by the Temple Butte unconformity (Beus 1989, 2003). Subsequently, basement rocks were buried by 2.5–3.5 km during the Mesozoic (McKee, 1951; Hintze, 1980; Molenaar, 1983; Billingsley et al., 1987; Blakey and Middleton, 2012) before being re-exhumed during the Laramide and by incision of Grand Canyon. Precise, quantitative constraints on the timing, duration and temperatures during burial are difficult to justify based on geologic and geochemical evidence. Temperatures during burial reheating are required to have been sufficiently high to cause substantial diffusive loss of previously-accumulated radiogenic  $^4\text{He}$  since (U–Th)/He ages are younger than 100 Ma and show no correlation with [eU] (Flowers et al., 2008; Flowers and Farley, 2012, 2013). However, ages younger than 100 Ma do not necessarily require complete annealing of radiation damage. Reset fission track ages across the Colorado Plateau highlight that peak temperatures were greater than 100 °C during maximum burial (Dumitru et al., 1994; Naeser et al., 2001; Kelley et al., 2001). However as there is a discrepancy between time-temperature paths derived from fission track and apatite (U–Th)/He analyses, we focus on the limits of precision of only the apatite (U–Th)/He and discuss the fission track data below.

##### 4.3. Inversion of $^4\text{He}/^3\text{He}$ data

In order to explore the temperature sensitivity of the  $^4\text{He}/^3\text{He}$  data from crystal CP06-69D, we infer a thermal history using non-linear inverse methods. We use a simple time-temperature path to parameterize the thermal history, greatly reducing the number of parameters which we infer during the inversion, yet maintaining the flexibility to describe both the young and old canyon models. In addition, correlations between the degree of radiation damage annealing during reheating and the sensitivity of the data to temperature within the last 70 Ma can be readily assessed.

In the simple parameterization, all time-temperature paths begin at 550 Ma and remain at surface temperatures (20 °C) until ~350 Ma (Fig. 4). This early section of the time-temperature path

represents the near surface conditions of the Temple Butte unconformity (Beus, 1989, 2003). The time-temperature path between 350 Ma and the present day is parameterized with six model parameters: temperature between  $t_1$  and  $t_2$  is equal to  $T_1$ ; temperature between  $t_3$  and  $t_4$  is equal to  $T_2$ . An additional constraint is imposed at 20 °C at the present day reflecting modern surface temperatures. A specific time-temperature path is linearly interpolated between (350 Ma, 20 °C) and ( $t_1, T_1$ ) and between ( $t_2, T_1$ ) and ( $t_3, T_2$ ) and also between ( $t_4, T_2$ ) and (0 Ma, 20 °C), Fig. 4.

We use the neighborhood algorithm (NA) (Sambridge, 1999a, 1999b) to determine optimum values of the model parameters and the uncertainties associated with the time-temperature history. This approach has been employed extensively for non-linear inverse problems in thermochronometry (Herman et al., 2007; Valla et al., 2010; Braun et al., 2011), and is not described here in detail. The NA is divided into two stages. In the first stage, the sampling stage, samples are drawn from the multidimensional parameter space for combinations of model parameters that minimize the difference between the observed  $^4\text{He}/^3\text{He}$  data and model predicted data. We only analyze the  $^4\text{He}/^3\text{He}$  data to isolate the effects of these data alone. The misfit value is,  $\phi$ ,

$$\phi = \frac{1}{N} \sum_{i=1}^N \left( \frac{R_{\text{pred},i} - R_{\text{obs},i}}{R_{\text{error},i}} \right)^2 \quad (1)$$

where  $R = R_{\text{step}}/R_{\text{bulk}}$ . If the predicted uncorrected age is outside of the range of measured uncorrected ages (from 45 to 75 Ma), then  $f$  is set to a large misfit value (1000). We do not attempt to fit a specific age because the apparent age of the crystal is unknown. The search stage was performed on a high performance cluster and 1500 forward simulations were performed. The second stage, the appraisal stage, provides estimates of the probability and covariance of the model parameters from the models collected during the search stage. The likelihood function used to compute the posterior probability density function (PPD) of parameter space is:

$$L = \exp\left(-\frac{\nu}{2}\phi\right) \quad (2)$$

where  $\nu$  is the number of data minus the independently constrained model parameters. The second stage produces an ensemble of time-temperature paths such that the density of paths through regions of parameter space is proportional to the posterior probability density function.

#### 4.4. Inferred time-temperature paths

The result of the inversion described above is presented as a 2D synoptic probability density plot (Glotsbach et al., 2011; Braun et al., 2011; Fillon and van der Beek, 2012), where the color relates to probability (Fig. 5A). The time-temperature space is divided into  $150 \times 150$  pixels and the normalized frequency of paths crossing a specific pixel provides the posterior probability. Results highlight that when incorporating uncertainty in burial conditions, time-temperature paths that are consistent with an old canyon model are almost equally probable as are time-temperature paths consistent with a young canyon model (Fig. 5A). Ultimately, this reduced resolving power of the  $^4\text{He}/^3\text{He}$  data, relative to the results of Flowers and Farley (2012), is due to the possibility of incomplete annealing of radiation damage during burial that results in variable (i.e., uncertain) temperature sensitivity of the sample since  $\sim 80$  Ma.

In order to further explore the temperature sensitivity of the  $^4\text{He}/^3\text{He}$  data, we assess correlations amongst model parameters. We select two regions of parameter space and all paths in the posterior ensemble that pass through these regions to highlight these

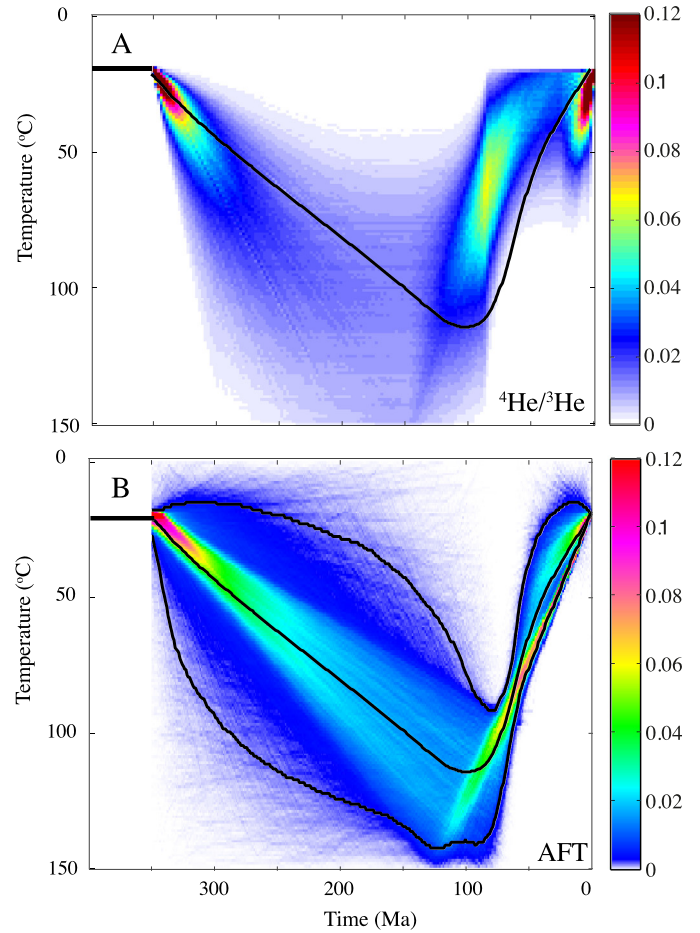


**Fig. 5.** Inferred time-temperature history for basement of Western Grand Canyon. (A) Synoptic probability density plot of time-temperature history for Western Grand Canyon inferred from the analysis of only  $^4\text{He}/^3\text{He}$  measurements combined with the spatial distribution of eU concentrations for sample CP06-69D. The color at a specific time temperature location defines the probability that the sample was at this temperature at this time. The region of high probability at 350 Ma and 20 °C is due to the imposed constraint representing the Temple Butt unconformity, the data cannot resolve temperature at this time. Similarly, the region of high probability at 0 Ma and 20 °C is due to the imposed present day temperature constraint. (B) Probability density plot of time-temperature space for Western Grand Canyon inferred from the analysis of only AFT data for sample GC63 (Lee et al., 2013) using QQt (Gallagher, 2012). The upper and lower black lines show the 95% credible interval (Bayesian equivalent to the 95% confidence interval). The central black line shows the expected model, which is the weighted average of the posterior ensemble. For reference, the solid curve shown in (A) is the same as the central curve in (B). (For interpretation of the references to color in this figure legend, the reader is referred to the web version of this article.)

correlations and produce conditional probability density functions all paths that pass through a time-temperature constraint consistent with: (1) a young canyon model (Fig. 6A); (2) an old canyon model (Fig. 6B). Here the colors relate to the conditional probability of time-temperature space given that the crystal passed through specific regions of time-temperature space. The correlation analysis highlights that paths that pass through region 1 are more likely to pass through relatively low temperatures during reheating (Fig. 6A). Conversely, paths that experience higher temperatures during reheating are more likely to be consistent with old canyon scenarios. For a given duration of burial, at low temperatures previously accumulated radiation damage is predicted to be retained whereas at higher temperatures radiation damage is annealed. Therefore, for lower burial temperatures, the  $^4\text{He}/^3\text{He}$  data are generally more consistent with higher temperatures after peak burial, whereas for higher burial temperatures, the  $^4\text{He}/^3\text{He}$  data are consistent with lower temperatures after burial. Finally,

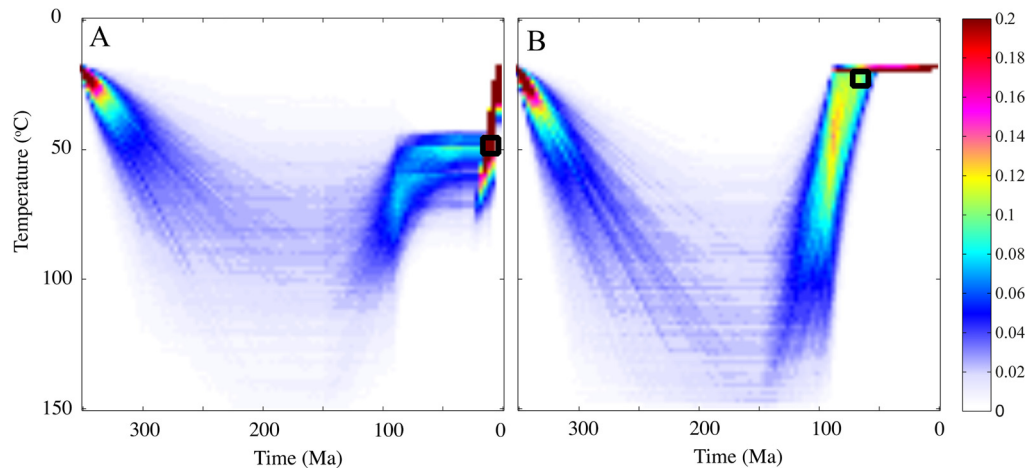


**Fig. 6.** Correlation analysis of the posterior probability density function constrained by apatite  $^4\text{He}/^3\text{He}$  data. (A) Conditional PDF given the condition that the crystal passed through a time-temperature constraint (indicated by the black box) indicative of a young canyon model. (B) Conditional PDF given that the crystal passed through a time-temperature constraint (black box) indicative of an old canyon model. Results highlight that  $^4\text{He}/^3\text{He}$ -based time-temperature solutions consistent with both the young and old canyon models are sensitive to specific details of the burial temperatures and durations. (For interpretation of the references to color in this figure, the reader is referred to the web version of this article.)

there is considerable overlap between the two clusters of paths reflecting uncertainty associated with the assumed (U–Th)/He age of the sample and analytical noise in the  $^4\text{He}/^3\text{He}$  data.

#### 4.5. Inconsistency with fission track data

There has been considerable fission track work across the Colorado Plateau that constrains burial temperatures (Dumitru et al., 1994; Naeser et al., 2001; Kelley et al., 2001). Here we consider published fission track data from the sample closest to the analyzed  $^4\text{He}/^3\text{He}$  crystal of Flowers and Farley (2013) to avoid the potential effects of differential cooling between different portions of the canyon (Karlstrom et al., 2014). We focus on apatite fission track data from sample number GC86 (Lee et al., 2013) which is <50 km along the river from sample CP06-69. The central fission track age for this sample is  $62.8 \pm 4.0$  Ma and the mean track length is  $13 \pm 1.65$   $\mu\text{m}$ . These data, along with (U–Th)/He from the same sample, were analyzed by Lee et al. (2013) using the Hefty program (Ketchum, 2005). They concluded that the data were consistent with a ‘young’ Western Grand Canyon model. To interrogate the temperature sensitivity of the apatite fission track system alone in this geologic setting, here, we solely analyze the fission track data.

In order to infer the probability that the sample was at a specific temperature at a specific time in the past, we use QTQt (Gallagher, 2012). QTQt exploits a reversible jump Markov Chain Monte Carlo (rjMCMC) algorithm (Green, 1995) to simultaneously sample parameter space and determine the complexity of the time-temperature path. The rjMCMC algorithm is initialized with a time-temperature path that randomly samples parameter space. A new model is proposed based on a perturbation from the current model, and is accepted or rejected based on an acceptance criterion. This acceptance criterion favors models that reduce data misfit yet the criterion penalizes models that are overly complex. Occasionally, models will be accepted that increase data misfit or complexity and this ensures that parameter space is sampled. Once a model is accepted, this model replaces the current model and a new model is once again generated as a perturbation of the current model. This process is typically repeated 10,000 s of times. Accepted models are asymptotically distributed according to the target distribution. They are saved and combined and this ensemble approximates the posterior probability density function [see Gallagher (2012) for further information].

We analyze sample GC86 using QTQt with a prior uniform distribution for time-temperature space between 0–550 Ma and 0–150 °C. We constrain the time-temperature path from 550 Ma to 350 Ma at surface temperatures of 20 °C. 20,000 time-temperature paths were simulated and the results of the analysis are shown in Fig. 5B. The expected history, Fig. 5B, produces a fission track age of 62.7 (compared with a measured age of  $62.8 \pm 4.0$  Ma) and a track length distribution of  $12.87 \pm 0.34$   $\mu\text{m}$  (compared to  $13 \pm 1.65$   $\mu\text{m}$ ). The results highlight that the FT data require cooling at 90 Ma followed by cooling to <100 °C by 75 Ma. This result is similar to the result obtained by Lee et al. (2013), and is inconsistent with an old canyon model. Differences between the result presented in Fig. 5B and the result obtained by Lee et al. (2013) are due to the exclusion of (U–Th)/He data in the current analysis. Due to the different model parameterizations used in the two different approaches outlined above, the absolute values of the probabilities in Figs. 5A and 5B cannot be directly compared with one another, although the relative patterns of probability can. The thermal paths constrained by existing apatite  $^4\text{He}/^3\text{He}$  and fission track data from this region of Grand Canyon are clearly inconsistent with one another. Since the thermal paths at this location necessarily have to be consistent, this result indicates that one or both of these systems is insufficiently understood.

#### 5. Further implications

We have shown that in cases other than those solely involving decreasing temperatures, the temperature sensitivity of the (U–Th)/He system depends strongly on specific details of a sample’s entire thermal history, particularly in applications of  $^4\text{He}/^3\text{He}$  thermochronometry. Uncertainty in the timescale and magnitude of reheating during burial will result in unknown He diffusion kinetics and thus poor constraints on the most recent phase of exhumation. The effects of reheating is particularly important for the (U–Th)/He system as variations in the duration of, or peak temperature during, reheating leads to variations in the degree of radiation damage annealing. The degree of radiation damage can, in turn, modify the temperature sensitivity of the (U–Th)/He system by 10 s of degrees C. Therefore, imposing constraints on permissible time-temperature paths during inverse modeling can lead to conclusions that are not obviously related to the constraints. In turn, analysis of correlations between different parts of parameter space may be required. This could involve imposing constraints to test the effects

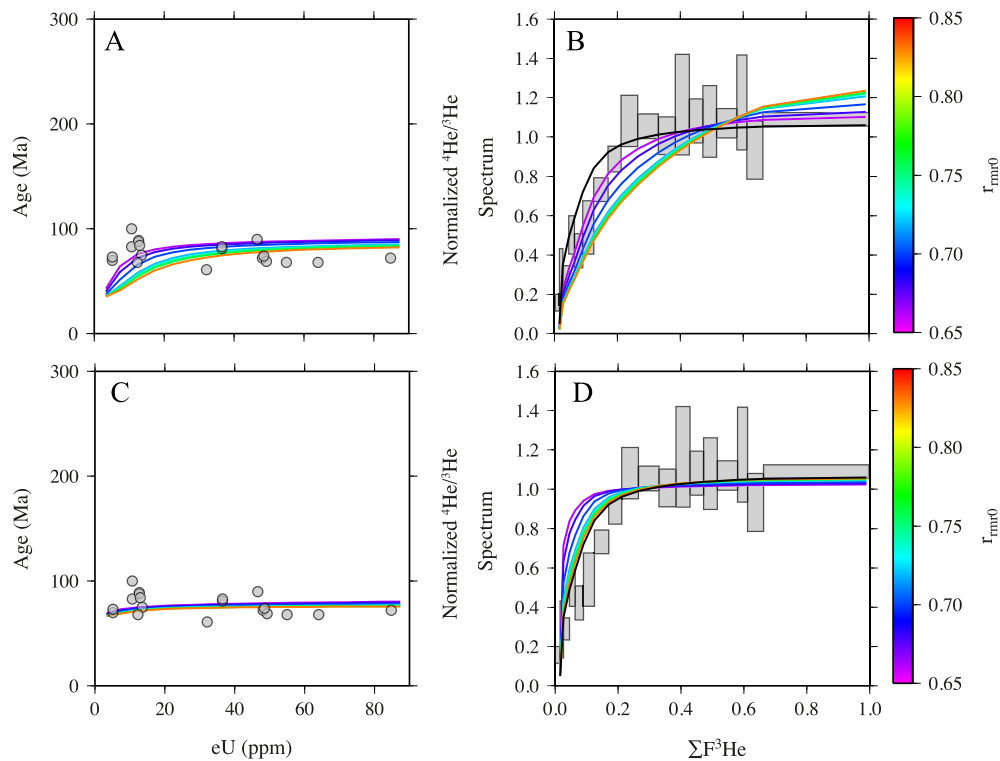


**Fig. 7.** Sensitivity of (U–Th)/He and  $^4\text{He}/^3\text{He}$  thermochronometers to variations in the assumed  $r_{mr0}$  parameter within RDAAM. The form of the time–temperature path used for these calculations is as in Fig. 2, however the peak temperature is set to 115 °C. The parameter  $r_{mr0}$ , which effectively controls the resistance of alpha recoil damage to annealing (hence the temperature dependence of its evolving effect on  $^4\text{He}$  diffusivity), is modified between simulations. (A) variations in the eU–age relationship due to systematically varying  $r_{mr0}$  for the first reference path. (B) effects on the normalized  $^4\text{He}/^3\text{He}$  spectrum due to varying  $r_{mr0}$  for the first reference path. (C) and (D) show the equivalent results for the second reference path. (For interpretation of the references to color in this figure legend, the reader is referred to the web version of this article.)

of these constraints during the search stage or through the analysis of the posterior probability density function, as carried out here.

In the Grand Canyon example, the apatite  $^4\text{He}/^3\text{He}$  data indicate that the crystal resided at temperatures that are characteristic of closed system behavior of the (U–Th)/He system (Flowers and Farley, 2012). However, due to the effects of radiation damage, the temperatures of transition from open to closed system behavior is variable depending on conditions during burial, and is therefore uncertain. Beginning time–temperature models at ~90 Ma requires old canyon solutions since complete annealing of previously accumulated radiation damage is implicitly assumed under that condition. Thus, with zero damage and highest  $^4\text{He}$  diffusivity (i.e., lowest  $T_c$ ) assumed at ~90 Ma, the  $^4\text{He}/^3\text{He}$  data require very low (20 °C) temperatures since ~80 Ma. However, if time–temperature models are permitted to begin prior to the peak burial conditions inferred from the AFT data, then the damage accumulation and annealing both before and during burial will influence the temperature sensitivity of the (U–Th)/He system, as discussed above. The effects of incomplete annealing of radiation damage cause the transition between open and closed system behavior to occur at higher temperatures during subsequent canyon incision. Therefore, the  $^4\text{He}/^3\text{He}$  data are also consistent with models involving long durations at intermediate temperatures (e.g., 40 °C) since 80 Ma, which is consistent with young canyon models. However, this leads to an age–[eU] correlation, which is not observed in the Western Grand Canyon dataset (Flowers and Farley, 2013). In addition, incomplete annealing of radiation damage requires that temperatures were low during burial reheating, in contrast to temperatures (>115 °C) constrained from the analysis of fission track data (Dumitru et al., 1994; Naeser et al., 2001; Kelley et al., 2001; Lee et al., 2013).

A thermal path that is internally consistent with both apatite  $^4\text{He}/^3\text{He}$  and AFT data from this geologic setting would require

decoupling RDAAM from the model of fission track annealing. In absence of empirical data and an adequate physical theory, RDAAM effectively assumes that the kinetics of alpha recoil damage annealing and its control on  $^4\text{He}$  diffusivity can be described by a function that was independently calibrated for fission track annealing in apatite (Flowers et al., 2009). However, the rate of annealing of alpha recoil damage is not well calibrated (Chaumont et al., 2002) and may depend on the type of radiation damage (Ritter and Märk, 1986). In geologic settings involving burial heating, uncertainty in the kinetics of damage annealing will therefore lead to significant uncertainty in evolution of  $^4\text{He}$  diffusivity, hence in post-burial exhumation. If, for example, the annealing of alpha recoil damage (and the resultant effects on  $^4\text{He}$  diffusivity) occurs at a lower rate than the annealing of fission tracks at a given temperature, then the recoil damage could be only partially annealed during burial (predicting lower  $^4\text{He}$  diffusivity after 80 Ma) while fission tracks would be completely annealed. Slight modifications in the annealing kinetics of radiation damage would significantly change the sensitivity of apatite  $^4\text{He}/^3\text{He}$  data to temperatures during and after burial heating. Likewise, similar inaccuracies may exist in the apatite fission track systematics; any errors in the assumed kinetics of fission track annealing would directly influence an inferred temperature during burial (e.g. Ketcham et al., 2007).

For example, if parameters in RDAAM are slightly varied, the evolution in temperature sensitivity of the (U–Th)/He system changes. The fission track annealing model accounts for grains with variable annealing kinetics (Ketcham et al., 2007). The key parameter in RDAAM describing resistance to annealing is  $r_{mr0}$ , which is the reduced length of a resistant apatite to annealing at the conditions where the less resistant apatite becomes totally annealed (Ketcham et al., 2007). Therefore, changing the parameter  $r_{mr0}$  in RDAAM provides a means to modify the annealing rate of radiation damage as determined by Gautheron et al. (2013). This

parameter has been observed to vary between 0.6 and 0.86 in natural apatite (Ketcham et al., 2007), which means uncertainty in this parameter also needs consideration. To explore this uncertainty, we use the reference time-temperature paths from Section 3.1.1 with a peak temperature set to 115 °C and ran experiments modifying  $r_{mr0}$  (Fig. 7). All other parameters in RDAAM are held constant.

The results highlight that by reducing the value of  $r_{mr0}$ , i.e., effectively making alpha recoil damage and its effect on  $^4\text{He}$  diffusivity more resistant to annealing than fission track annealing, radiation damage is maintained while fission tracks are completely annealed. In the case of Western Grand Canyon data, the predicted age-[eU] relationships and  $^4\text{He}/^3\text{He}$  release spectra are in closer agreement with the observed (U–Th)/He ages and  $^4\text{He}/^3\text{He}$  data, Figs. 7A and 7B. For comparison, the predicted age-[eU] relationship and normalized  $^4\text{He}/^3\text{He}$  spectrum are also shown for the second reference path, Figs. 7C and 7D. This highlights that similar age-[eU] relationships and normalized  $^4\text{He}/^3\text{He}$  spectrum results can be obtained for old and young canyon models by modifying the resistance of radiation damage to annealing. However, the large range of probable temperatures during the last ~70 Ma (i.e., Fig. 5A) persists, due to the uncertainties in burial conditions discussed above.

This approach used to modify the annealing rate of alpha recoil damage and its effect on  $^4\text{He}$  diffusivity in apatite is only intended for illustrative purposes, but indicates that additional work is required to test and refine the parameters in RDAAM and fission track annealing. At present, there are few studies that test for internal consistency between thermal constraints based on apatite (U–Th)/He and FT data (e.g., Green et al., 2006; Flowers et al., 2009; Flowers and Kelley, 2011) and only one that empirically quantifies the effects of damage annealing on  $^4\text{He}$  diffusivity (Shuster and Farley, 2009). Future experimental work is therefore required to more precisely quantify the kinetics of alpha recoil damage annealing and the related control on  $^4\text{He}$  diffusivity in apatite.

## 6. Conclusions

We have shown that in geologic settings of sedimentary burial heating and subsequent exhumation, the interpretation of apatite  $^4\text{He}/^3\text{He}$  data, and quantitative constraints on, and uncertainty in, exhumation requires careful exploration of model parameters, including uncertainties in burial conditions. Such uncertainties suggest that existing apatite  $^4\text{He}/^3\text{He}$  data cannot resolve the timing of Grand Canyon incision unless additional constraints are included. This is because the extent of radiation damage accumulation and annealing can dramatically change the temperature sensitivity of the (U–Th)/He system to subsequent exhumation; therefore, the cooling signature of canyon incision is at the limit of resolution. Reheating during burial may not lead to complete annealing of radiation damage and thus results in uncertainty in the  $^4\text{He}$  retentivity of a given crystal. Even if the parameters defining radiation damage accumulation and annealing could be independently constrained, the range of  $^4\text{He}$  retentivity is difficult to quantify and this may limit the precision of an inferred time-temperature history. Increased understanding of He diffusion kinetics as a function of radiation damage and quantifying the kinetics of  $^4\text{He}$  diffusion for analyzed crystals could help distinguish between young canyon and old canyon models.

The Grand Canyon is a key location where the resolution limits of both the AFT and (U–Th)/He data have been tested. This natural laboratory has highlighted a discrepancy between time-temperature histories derived from the two systems, and suggests that previously unrecognized complexities exist in the current quantifications of fission track annealing and/or  $^4\text{He}$  diffusion kinetics in apatite. Part of this discrepancy may result from the fact

that the RDAAM is coupled to fission track annealing. Importantly, the RDAAM is constrained primarily by the correlation between  $^4\text{He}$  retentivity and calculated fission track density (Shuster et al., 2006; Shuster and Farley, 2009; Flowers et al., 2009). Therefore, the accumulation of the radiation damage component of the RDAAM is likely to be well constrained. However, there are very few datasets that constrain the annealing component of RDAAM. In turn, if the annealing of alpha recoil damage and its effect on  $^4\text{He}$  diffusivity in apatite is decoupled from existing models of fission track annealing, coexisting datasets for individual samples may be found to be more compatible with one another.

## Acknowledgements

We would like to thank G. Balco and R. Ickert for helpful discussions and A. Ault for discussing her observations that highlight the important role of  $r_{mr0}$ . The computations presented here were performed on the Brutus facility at ETH Zurich, Switzerland. This manuscript benefited from helpful reviews by A. Ault and an anonymous reviewer. This work has been supported by the Swiss National Science Foundation (P2EZP2\_148793), the Ann and Gordon Getty Foundation and the National Science Foundation (EAR-1347990).

## References

- Ault, A.K., Flowers, R.M., Bowring, S.A., 2009. Phanerozoic burial and unroofing history of the Western Slave Craton and Wopmay orogen from apatite (U–Th)/He thermochronometry. *Earth Planet. Sci. Lett.* 284 (1), 1–11.
- Beus, S.S., 1989. Devonian and Mississippian geology of Arizona. In: *Geologic Evolution of Arizona*. *Ariz. Geol. Soc. Dig.* 17, 287–311.
- Beus, S.S., 2003. Temple butte formation. In: Beus, S.S., Morales, M. (Eds.), *Grand Canyon Geology*. 2nd edition. Oxford University Press, pp. 107, 114.
- Billingsley, G., Huntoon, P., Breed, W., 1987. Geologic map of Capitol Reef National Park and vicinity, Emery, Garfield, Kane, and Wayne Counties, Utah. *Utah Geological and Mineral Survey Map 87*, scale 1: 62,500.
- Blakey, R.C., Middleton, L.T., 2012. Geologic history and paleogeography of Paleozoic and early Mesozoic sedimentary rocks, eastern Grand Canyon, Arizona. *Spec. Pap., Geol. Soc. Am.* 489, 81–92.
- Braun, J., Van der Beek, P., Valla, P., Robert, X., Herman, F., Glotzbach, C., Pedersen, V., Perry, C.P., Simon-Labric, T., Prigent, C., 2011. Quantifying rates of landscape evolution and tectonic processes by thermochronology and numerical modeling of crustal heat transport using PECUBE. *Tectonophysics* 524, 1–28.
- Chaumont, J., Soulet, S., Krupa, J., Carpena, J., 2002. Competition between disorder creation and annealing in fluorapatite nuclear waste forms. *J. Nucl. Mater.* 301 (2), 122–128.
- Dodson, M.H., 1973. Closure temperature in cooling geochronological and petrological systems. *Contrib. Mineral. Petrol.* 40, 259–274.
- Dorsey, R.J., Fluette, A., McDougall, K., Housen, B.A., Janecke, S.U., Axen, G.J., Shirvell, C.R., 2007. Chronology of Miocene–Pliocene deposits at Split Mountain Gorge, southern California: a record of regional tectonics and Colorado River evolution. *Geology* 35 (1), 57–60.
- Dumitru, T.A., Duddy, I.R., Green, P.F., 1994. Mesozoic–Cenozoic burial, uplift, and erosion history of the west-central Colorado Plateau. *Geology* 22 (6), 499–502.
- Ehlers, T.A., Farley, K.A., 2003. Apatite (U–Th)/He thermochronometry: methods and applications to problems in tectonic and surface processes. *Earth Planet. Sci. Lett.* 206, 1–2.
- Ehlers, T.A., Farley, K.A., Rusmore, M.E., Woodsworth, G.J., 2006. Apatite (U–Th)/He signal of large-magnitude accelerated glacial erosion, southwest British Columbia. *Geology* 34 (9), 765–769.
- Farley, K.A., 2000. Helium diffusion from apatite: general behavior as illustrated by Durango fluorapatite. *J. Geophys. Res.* 105 (B2), 2903–2914.
- Farley, K.A., Wolf, R.A., Silver, L.T., 1996. The effects of long alpha-stopping distances on (U–Th)/He ages. *Geochim. Cosmochim. Acta* 60, 4223–4229.
- Farley, K.A., Shuster, D.L., Watson, E., Wanser, K., Balco, G., 2010. Numerical investigations of apatite  $^4\text{He}/^3\text{He}$  thermochronometry. *Geochim. Geophys. Geosyst.* 11 (10), 1–18. <http://dx.doi.org/10.1029/2010GC003243>.
- Farley, K.A., Shuster, D.L., Ketcham, R.A., 2011. U and Th zonation in apatite observed by laser ablation ICPMS, and implications for the (U–Th)/He system. *Geochim. Cosmochim. Acta* 75 (16), 4515–4530.
- Faulds, J.E., Price, L.M., Wallace, M.A., 2001. Pre-Colorado River paleogeography and extension along the Colorado Plateau–Basin and Range boundary, northwestern Arizona. In: *Colorado River: Origin and Evolution: Grand Canyon, Arizona*. In: *Grand Canyon Assoc. Monogr.*, vol. 12, pp. 93–99.

- Fechtig, H., Kalbitzer, S., 1966. The diffusion of argon in potassium-bearing solids. In: Schaeffer, A., Zähringer, J. (Eds.), *Potassium Argon Dating*. Springer, pp. 68–107.
- Fillon, C., van der Beek, P., 2012. Post-orogenic evolution of the southern Pyrenees: constraints from inverse thermo-kinematic modelling of low-temperature thermochronology data. *Basin Res.* 24 (4), 418–436.
- Fillon, C., Gautheron, C., van der Beek, P., 2013. Oligocene–Miocene burial and exhumation of the Southern Pyrenean foreland quantified by low-temperature thermochronology. *J. Geol. Soc.* 170 (1), 67–77.
- Flowers, R., Farley, K., 2012. Apatite  $^4\text{He}/^3\text{He}$  and (U–Th)/He evidence for an ancient Grand Canyon. *Science* 338 (6114), 1616–1619.
- Flowers, R., Farley, K., 2013. Response to comments on “Apatite  $^4\text{He}/^3\text{He}$  and (U–Th)/He Evidence for an Ancient Grand Canyon”. *Science* 340 (6129), 143.
- Flowers, R., Wernicke, B., Farley, K., 2008. Unroofing, incision, and uplift history of the southwestern Colorado Plateau from apatite (U–Th)/He thermochronometry. *Geol. Soc. Am. Bull.* 120 (5–6), 571–587.
- Flowers, R.M., Ketcham, R.A., Shuster, D.L., Farley, K.A., 2009. Apatite (U–Th)/He thermochronometry using a radiation damage accumulation and annealing model. *Geochim. Cosmochim. Acta* 73 (8), 2347–2365.
- Flowers, R.M., 2009. Exploiting radiation damage control on apatite (U–Th)/He dates in cratonic regions. *Earth Planet. Sci. Lett.* 277 (1), 148–155.
- Flowers, R.M., Kelley, S.A., 2011. Interpreting data dispersion and inverted dates in apatite (U–Th)/He and fission-track datasets: an example from the US mid-continent. *Geochim. Cosmochim. Acta* 75 (18), 5169–5186.
- Gallagher, K., 2012. Transdimensional inverse thermal history modeling for quantitative thermochronology. *J. Geophys. Res., Solid Earth* 117 (B2), 2156–2202.
- Gautheron, C., Tassan-Got, L., Barbarand, J., Pagel, M., 2009. Effect of alpha-damage annealing on apatite (U–Th)/He thermochronology. *Chem. Geol.* 266 (3), 157–170.
- Gautheron, C., Barbarand, J., Ketcham, R.A., Tassan-Got, L., van der Beek, P., Pagel, M., Pinna-Jamme, R., Couffignal, F., Fialin, M., 2013. Chemical influence on  $\alpha$ -recoil damage annealing in apatite: implications for (U–Th)/He dating. *Chem. Geol.* 351, 257–267.
- Glottzbach, C., van der Beek, P.A., Spiegel, C., 2011. Episodic exhumation and relief growth in the Mont Blanc massif, Western Alps from numerical modelling of thermochronology data. *Earth Planet. Sci. Lett.* 304, 417–430.
- Green, P.F., Crowhurst, P.V., Duddy, I.R., Japsen, P., Holford, S.P., 2006. Conflicting (U–Th)/He and fission track ages in apatite: enhanced He retention, not anomalous annealing behaviour. *Earth Planet. Sci. Lett.* 250 (3), 407–427.
- Green, P.J., 1995. Reversible jump Markov chain Monte Carlo computation and Bayesian model determination. *Biometrika* 82 (4), 711–732.
- Herman, F., Braun, J., Dunlap, W.J., 2007. Tectonomorphic scenarios in the Southern Alps of New Zealand. *J. Geophys. Res., Solid Earth* 112 (B4), B04201.
- Hill, C.A., Ranney, W., 2008. A proposed Laramide proto-Grand Canyon. *Geomorphology* 102 (3), 482–495.
- Hintze, L., 1980. *Geologic map of Utah, 2 sheets, Utah Geol. Miner. Surv.*, 1:500,000.
- House, M.A., Wernicke, B.P., Farley, K.A., 1998. Dating topography of the Sierra Nevada, California, using apatite (U–Th)/He ages. *Nature* 396, 66–69.
- Howard, A., Dietrich, W., Seidl, M., 1994. Modeling fluvial erosion on regional to continental scales. *J. Geophys. Res.* 99, 13971–13986.
- Ingersoll, R.V., Grove, M., Jacobson, C.E., Kimbrough, D.L., Hoyt, J.F., 2013. Detrital zircons indicate no drainage link between southern California rivers and the Colorado Plateau from mid-Cretaceous through Pliocene. *Geology* 41 (3), 311–314.
- Karlstrom, K., Coblenz, D., Dueker, K., Ouimet, W., Kirby, E., Van Wijk, J., Schmandt, B., Kelley, S., Lazear, G., Crossey, L., et al., 2012. Mantle-driven dynamic uplift of the Rocky Mountains and Colorado Plateau and its surface response: toward a unified hypothesis. *Lithosphere* 4 (1), 3–22.
- Karlstrom, K.E., Timmons, J.M., 2012. Many unconformities make one Great Unconformity. *Spec. Pap., Geol. Soc. Am.* 489, 73–79.
- Karlstrom, K.E., Lee, J., Kelley, S., Crow, R., Young, R.A., Lucchitta, I., Beard, L.S., Dorsey, R., Ricketts, J.W., Dickinson, W.R., Crossey, L., 2013. Comment on apatite  $^4\text{He}/^3\text{He}$  and (U–Th)/He Evidence for an Ancient Grand Canyon. *Science* 340 (6129), 143.
- Karlstrom, K.E., Lee, J.P., Kelley, S., Shari, A., Crow, R.S., Crossey, L.J., Young, R.A., Lazear, G., Beard, L.S., Ricketts, J.W., Fox, M., Shuster, D.L., 2014. Formation of the Grand Canyon 5 to 6 million years ago through integration of older palaeocanyons. *Nat. Geosci.* 7, 239–244.
- Kelley, S.A., Chapin, C.E., Karlstrom, K.E., 2001. Laramide cooling histories of Grand Canyon, Arizona, and the Front Range, Colorado, determined from apatite fission-track thermochronology. In: *Colorado River: Origin and Evolution: Grand Canyon, Arizona*. In: Grand Canyon Assoc. Monogr., pp. 37–42.
- Ketcham, R.A., 2005. Forward and inverse modeling of low-temperature thermochronometry data. *Rev. Mineral. Geochem.* 58 (1), 275–314.
- Ketcham, R.A., Carter, A., Donelick, R.A., Barbarand, J., Hurford, A.J., 2007. Improved modeling of fission-track annealing in apatite. *Am. Mineral.* 92 (5–6), 799–810.
- Lee, J.P., Stockli, D.F., Kelley, S.A., Pederson, J.L., Karlstrom, K.E., Ehlers, T.A., 2013. New thermochronometric constraints on the Tertiary landscape evolution of the central and eastern Grand Canyon, Arizona. *Geosphere* 9 (2), 216–228.
- Lucchitta, I., 2013. Comment on “Apatite  $^4\text{He}/^3\text{He}$  and (U–Th)/He Evidence for an Ancient Grand Canyon”. *Science* 340, 143–147.
- Lucchitta, I., Jeanne, R.A., 2001. Geomorphic features and processes of the Shivwits Plateau, Arizona, and their constraints on the age of western Grand Canyon. In: *Colorado River: Origin and Evolution: Grand Canyon, Arizona*. In: Grand Canyon Assoc. Monogr., vol. 12, pp. 65–69.
- McKee, E.D., 1951. Sedimentary basins of Arizona and adjoining areas. *Geol. Soc. Am. Bull.* 62 (5), 481–506.
- Molenaar, C.M., 1983. Major depositional cycles and regional correlations of Upper Cretaceous Rocks, southern Colorado Plateau and adjacent areas. In: Reynolds, M.W., Dolly, E.D. (Eds.), *Mesozoic Paleogeography of West-Central United States: Denver, Colorado, Rocky Mountain Section*. Society for Sedimentary Geology, pp. 201–223.
- Moucha, R., Forte, A.M., Rowley, D.B., Mitrovica, J.X., Simmons, N.A., Grand, S.P., 2008. Mantle convection and the recent evolution of the Colorado Plateau and the Rio Grande Rift valley. *Geology* 36 (6), 439–442.
- Naeser, C., Duddy, I., Elston, D., Dumitru, T., Green, P., 2001. Fission-track analysis of apatite and zircon from Grand Canyon, Arizona. In: *Colorado River: Origin and Evolution, Grand Canyon National Park*. In: Grand Canyon Assoc. Monogr., Grand Canyon, Arizona, pp. 31–36.
- Powell, J.W., 1875. *Exploration of the Colorado River of the West and Its Tributaries*. U.S. Govt. Printing Office, Washington, D.C.
- Polyak, V., Hill, C., Asmerom, Y., 2008. Age and evolution of the Grand Canyon revealed by U–Pb dating of water table-type speleothems. *Science* 319 (5868), 1377–1380.
- Potochnik, A.R., 2001. Paleogeomorphic evolution of the salt river region: implications for Cretaceous–Laramide inheritance for ancestral Colorado river drainage. In: *Colorado River: Origin and Evolution: Grand Canyon, Arizona*. In: Grand Canyon Assoc. Monogr., pp. 17–22.
- Reiners, P.W., Brandon, M.T., 2006. Using thermochronology to understand orogenic erosion. *Annu. Rev. Earth Planet. Sci.* 34, 419–466.
- Ritter, W., Märk, T., 1986. Radiation damage and its annealing in apatite. *Nucl. Instrum. Methods Phys. Res., Sect. B, Beam Interact. Mater. Atoms* 14 (3), 314–322.
- Roberts, G., White, N., Martin-Brandis, G., Crosby, A., 2012. An uplift history of the Colorado Plateau and its surroundings from inverse modeling of longitudinal river profiles. *Tectonics* 31 (4), 1–25. <http://dx.doi.org/10.1029/2012TC003107>.
- Sambridge, M., 1999a. Geophysical inversion with a neighbourhood algorithm – I. Searching a parameter space. *Geophys. J. Int.* 138, 479–494.
- Sambridge, M., 1999b. Geophysical inversion with a neighbourhood algorithm – II. Appraising the ensemble. *Geophys. J. Int.* 138 (3), 727–746.
- Schildgen, T.F., Balco, G., Shuster, D.L., 2010. Canyon incision and knickpoint propagation recorded by apatite  $^4\text{He}/^3\text{He}$  thermochronometry. *Earth Planet. Sci. Lett.* 293 (3), 377–387.
- Shuster, D.L., Farley, K.A., 2004.  $^4\text{He}/^3\text{He}$  thermochronometry. *Earth Planet. Sci. Lett.* 217, 1–2.
- Shuster, D.L., Ehlers, T.A., Rusmore, M.E., Farley, K.A., 2005. Rapid glacial erosion at 1.8 Ma revealed by  $^4\text{He}/^3\text{He}$  thermochronometry. *Science* 310, 1668–1670.
- Shuster, D.L., Flowers, R.M., Farley, K.A., 2006. The influence of natural radiation damage on helium diffusion kinetics in apatite. *Earth Planet. Sci. Lett.* 249 (3), 148–161.
- Shuster, D.L., Farley, K.A., 2009. The influence of artificial radiation damage and thermal annealing on helium diffusion kinetics in apatite. *Geochim. Cosmochim. Acta* 73 (1), 183–196.
- Shuster, D.L., Cuffey, K.M., Sanders, J.W., Balco, G., 2011. Thermochronometry reveals headward propagation of erosion in an Alpine landscape. *Science* 332 (6025), 84–89.
- Spencer, J.E., Pearthree, P.A., 2001. Headward erosion versus closed-basin spillover as alternative causes of Neogene capture of the ancestral Colorado River by the gulf of California. In: *The Colorado River: Origin and Evolution: Grand Canyon, Arizona*. In: Grand Canyon Assoc. Monogr., vol. 12, pp. 215–219.
- Spotila, J.A., Buscher, J.T., Meigs, A.J., Reiners, P.W., 2004. Long-term glacial erosion of active mountain belts: example of the Chugach–St. Elias Range, Alaska. *Geology* 32 (6), 501–504.
- Valla, P.G., Herman, F., van der Beek, P.A., Braun, J., 2010. Inversion of thermochronological age–elevation profiles to extract independent estimates of denudation and relief history – I: Theory and conceptual model. *Earth Planet. Sci. Lett.* 295 (3–4), 511–522.
- Valla, P.G., Shuster, D.L., van der Beek, P.A., 2011. Significant increase in relief of the European Alps during mid-Pleistocene glaciations. *Nat. Geosci.* 4 (10), 688–692.
- Wernicke, B., 2011. The California River and its role in carving Grand Canyon. *Geol. Soc. Am. Bull.* 123 (7–8), 1288–1316.
- Young, R.A., 1989. Paleogene–Neogene deposits of western Grand Canyon, Arizona. In: *Geology of Grand Canyon, Northern Arizona (with Colorado River Guides): Lee Ferry to Pierce Ferry, Arizona*, pp. 166–174.
- Young, R.A., 2001. The Laramide–Paleogene history of the western Grand Canyon region: setting the stage. In: *Colorado River: Origin and Evolution: Grand Canyon, Arizona*. In: Grand Canyon Assoc. Monogr., pp. 7–15.
- Young, R.A., 2008. Pre-Colorado River drainage in western Grand Canyon: Potential influence on Miocene stratigraphy in Grand Wash Trough. *Spec. Pap., Geol. Soc. Am.* 439, 319–333.
- Zeitler, P., Herczeg, A., McDougall, I., Honda, M., 1987. U–Th–He dating of apatite: a potential thermochronometer. *Geochim. Cosmochim. Acta* 51 (10), 2865–2868.